Chapter 3

Off-axis digital holographic microscope for quantification of blood cells

A traditional bright field microscope can only provide 2D intensity information of the biological cells and other micro-objects [3-4]. An intensity image is a map of spatial variation in absorption/reflection. To have high contrast images, there should be appreciable variation in intensity between the object of interest and the medium surrounding it. Also to identify different portions of the object there should be intensity variation across the object of interest. But unfortunately, most of the biological cells are transparent in nature and do not produces noticeable change in amplitude of visible electromagnetic radiation passing through them which results in poor contrast of intensity images [3-4]. Bright filed microscopes provides object information only at a single object plane. To acquire information from different object planes a mechanical movement, to focus on to different layers of object, is also required. Image contrast can be improved by using chemical agents, which gets attached to the cells and increases the absorption cross section leading to high intensity difference between the cells and their background [3-6]. This is usually referred as staining or labeling or tagging. But since this process involves chemical treatment of cells, it may alter their life cycle and morphology. Even though bright field microscopes provide important cell information depending upon their absorption profile they fail to provide any cell morphology information, which is important from point of view of cell characterization and identification.

Confocal microscopy, which is a scanning technique (cell is scanned in the lateral and axial direction usually with a laser beam) can also provide high contrast cell images along with their depth/thickness information [6]. Since it is a scanning technique, it cannot be termed as a single shot method. Single shot methods provide thickness information of the whole cell from a single exposure. Confocal microscopes requires multiple exposures for reconstruction of thickness profile of the whole cell as well as the technical expertise to achieve this. It should also be noted that confocal microscopes in many cases require a labelling agent.

Can high contrast 3D imaging of cells be achieved in a simpler way? The answer lies in the phase of the probe beam interacting with the cells. The phase of the probe beam, which depends upon

the distance traversed by it through the cell is very sensitive to the optical thickness variations of the cell and can be expressed as [7, 11-12, 17]

$$\phi_C(x,y) = \frac{2\pi}{\lambda} n_C\, h(x,y) \tag{3.1}$$

where λ is the vacuum wavelength of the probe beam and n_C is the refractive index of the cell and h its thickness. If intensity values can be assigned to the phase values, it will provide high contrast images of low absorbing specimen (Fig. 3.1) [17]. The technique of assigning different intensity values to different phase of the probe beam containing object information is called as phase contrast imaging [3-4, 7, 11-12, 17].

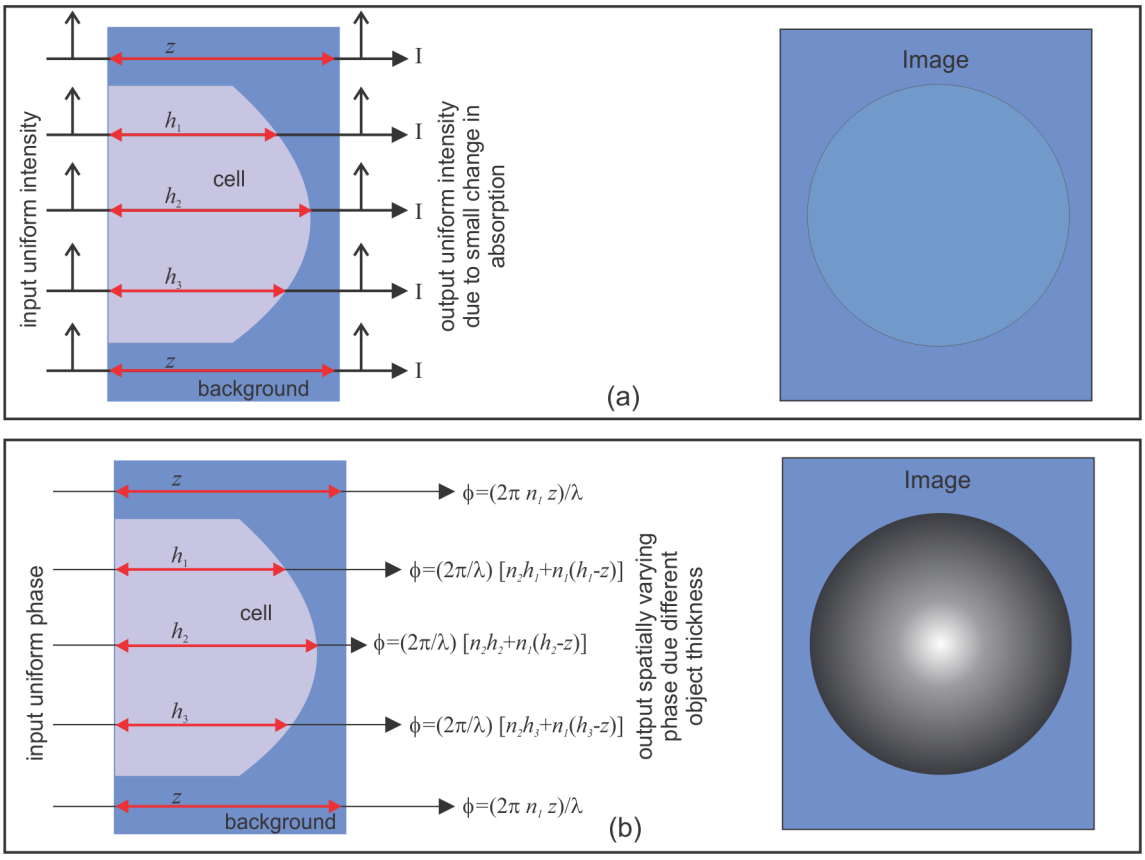

Fig. 3.1: (a) Imaging intensity of the probe beam leads to low contrast images of unstained sample since the absorption is less. (b) One the other hand imaging the phase of the probe beam leads to high contrast images of unstained samples since the probe beam phase changes appreciably even for small thickness (of the order of λ of the probe beam used) variation.

In phase contrast techniques, phase information is captured by the superposition of two light waves leading to interference. Usually, as shown in Fig. 3.1b, phase of the probe beam is converted into an intensity value and displayed. This can be termed as a qualitative technique [11-12]. Instead, if the phase of the probe beam is accessible, then according to Eq. (3.1) it can be used to compute the thickness profile of the object leading to Quantitative Phase Imaging (QPI). Interference techniques [13] including holography [14] are commonly used for QPI, where the probe beam is superposed with a reference leading to creation of interference fringes, which contains the object phase information as a modulation of the fringes [7, 16-99, 106-107]. Latest 3D interference microscopes record the interferograms on digital arrays and numerically process them to extract he object phase information [7, 17, 16-199, 106-107]. Digital holographic interferometric microscopy (DHIM) is one of the advance imaging technique that offers real-time imaging of phase objects such as living cells and quantitative measurements of their physiological parameters [16-107]. DHIM techniques allows one to investigate living cells without staining or labeling them [20-32, 38, 40-42, 44-53, 55-61, 63-99]. DHIM makes it possible to measure cell parameters such as cell thickness, surface area, volume, fluctuations, refractive index, motility etc., which is not possible with bright-field microscopy. These techniques not only allow us to plot the thickness profile of cells (cell morphology) but also allow us to study cell dynamics (time evolving cell morphology).

This chapter describes the design and fabrication of two-beam off-axis Digital Holographic Interference Microscopes based on Mach-Zehnder interferometer geometry [63] and its application in 3D imaging of human red blood cells. Blood cell parameters based on its morphology are extracted using the developed microscope and were used to characterize them leading to their discrimination and disease identification [63, 72-73].

3.1 Digital holography

As mentioned in the previous section, holographic imaging requires superposition of an object and a reference beam (Fig. 3.2) leading to creation of interference fringes or holograms. Holograms is a record of both phase and amplitude of the object wavefront [14, 18-19]. These interference fringes carry the object information as a modulation of the fringes itself. In the case of digital holography, the holograms are constructed optically, usually using a laser source and recorded suing a digital array [18]. For the superposition of the object beam given by $U_O = O \exp(i\phi_O)$ and

reference beam given by $U_R = O \exp(i\phi_O)$, the modulated intensity pattern recorded by the detector array can be written as

$$I(x,y) = |U_O + U_R|^2 = I_O + I_R + OR^* \exp\left[i(\phi_O - \phi_R)\right] + O^* R \exp\left[-i(\phi_O - \phi_R)\right] \quad (3.2)$$

where O and R are the scalar amplitudes of object and reference waves respectively and ϕ_O and ϕ_R are the phases of object and reference waves respectively. It can be seen from Eq. (3.2) that the carrier fringe system (which exists before the introduction of the object) gets modified in the regions where object exist.

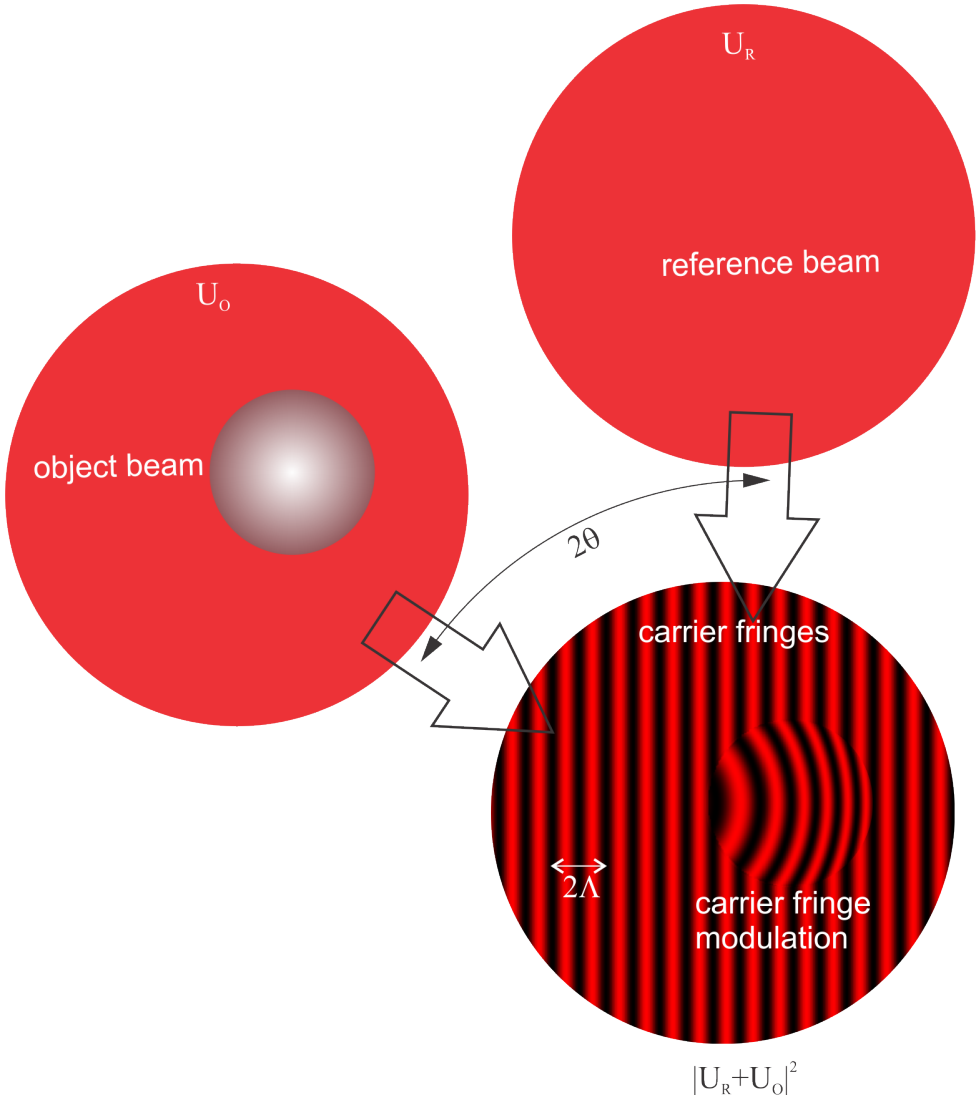

Fig. 3.2: Superposition of object and reference beams leads to formation of interference fringes or holograms. If there is no object in present, the superposition will lead to creation of carrier fringes. Fringes in the region where object existed gets modulated due pathlength/phase change.

Holograms/interferogram shown in Fig. 2.2 is a series of dark and bright bands which can be viewed as a grating created by two beams interfering at angle 2θ. The pitch of the grating is decided by this angle of interference and is given by [13]

$$\Lambda = \frac{\lambda}{2\sin(\theta)} \tag{3.3}$$

If object beam is removed and the grating (interference pattern) is illuminated by the reference beam incident at the same angle that was used to record it, then it should scatter light along the path of the object beam according to Eq. (3.2).

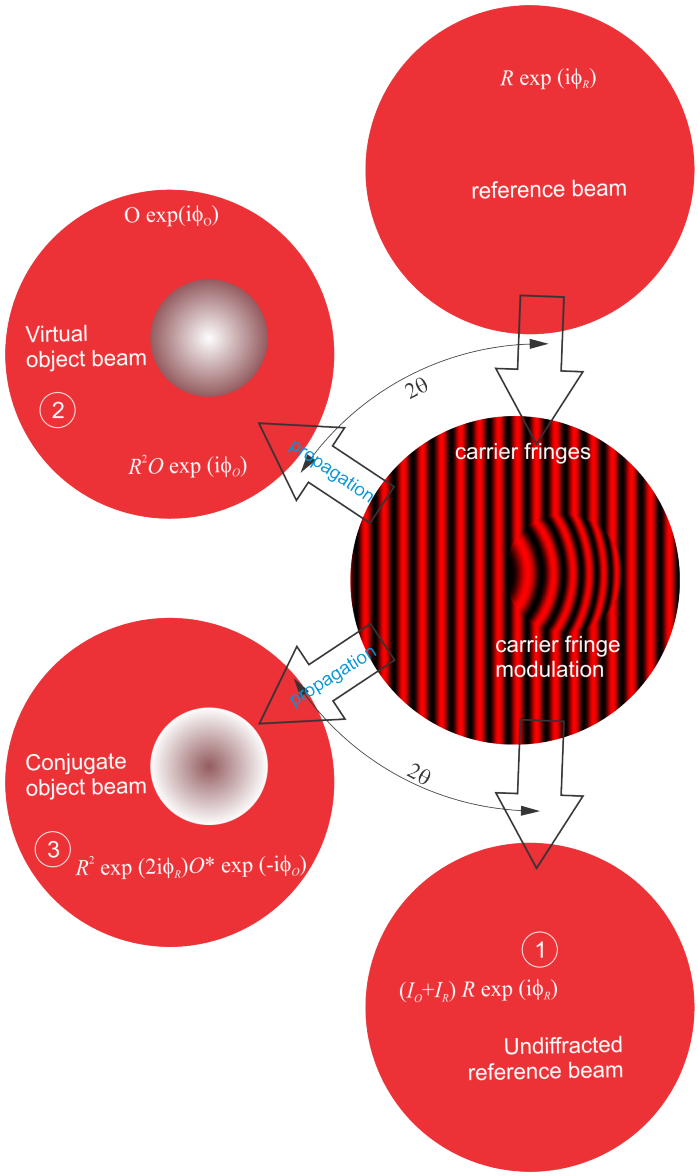

Fig. 3.3: Re-illumination of the hologram by replica of the reference beam.

Since the fringe pattern is modulated because of object, the scattered beam will have phase information of the object along the direction of the object beam (Fig. 3.3). So optical hologram reconstruction involves illuminating the recorded hologram by an exact replica of the object beam. The mathematical equivalent is multiplying the hologram given by Eq. (3.2) by the mathematical equivalent of the reference beam.

$$I\,R\exp\left(i\phi_R\right)=\left(I_O+I_R\right)R\exp\left(i\phi_R\right)+R^2O\exp\left(i\phi_O\right)+R^2\exp\left(2i\phi_R\right)O^*\exp\left(-i\phi_O\right) \tag{3.4}$$

In Eq. (3.4), first term represents the reference beam multiplied by the constant factor. It is the portion of the reference beam passing undiffracted (marked as 1 in Fig. 3.3) after interaction with the hologram. Second term is an exact replica of the object beam (marked as 2 in Fig. 3.3) multiplied by a constant, which provides a virtual object beam. Third terms provide the conjugate of the object beam (marked as 3 in Fig. 3.3) multiplied by a phase factor. If the reference beam had a plane wavefront, then the phase term in the third term becomes a constant and, in the case, where the phase of the reference beam is zero it becomes a constant real number, thereby providing just the complex conjugate of the object beam.

In digital holography, numerical reconstruction of hologram starts by the illumination of the recorded digital version of the hologram by a digital replica of the reference wavefront. From Eq. (3.4) this action leads to creation of three beams. The scattered/diffracted reference wave at the hologram plane needs to be propagated to the object (either virtual or conjugate) plane [28, 100-104]. The complex amplitude distribution at the hologram plane (z=0) arising because of its illumination by reference beam (Fig. 3.4) is

$$U_H\left(x,y,z=0\right)=R\exp\left(i\phi_R\right)I\left(x,y\right) \tag{3.5}$$

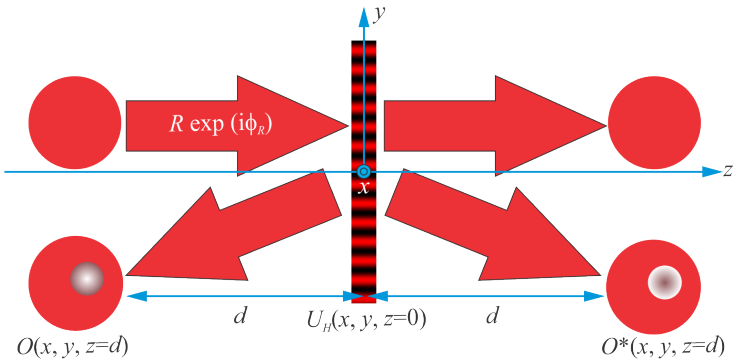

Fig. 3.4: Generation of different diffracted beams and their direction when hologram is illuminated by reference beam.

Now a wavefront scattered by an object represents the spatial frequency spectrum of the object. In this case the since the hologram, which is an interference pattern, can be considered as a sinusoidal grating, the complex amplitude distribution after the hologram, has three distinct terms (Fig. 3.5). This needs to be propagated to the object plane. The numerical propagation from hologram plane to image plane can be achieved using diffraction integral [28, 104-106]. In the case of short distance propagations angular spectrum propagation (ASP), in which the filtered spatial frequency spectrum of the scattered reference field is propagated to the object plane is more suitable [55, 60, 63, 106]. In all the developed holographic microscopy techniques discussed in the thesis, this approach is utilized for numerical processing of holograms [106].

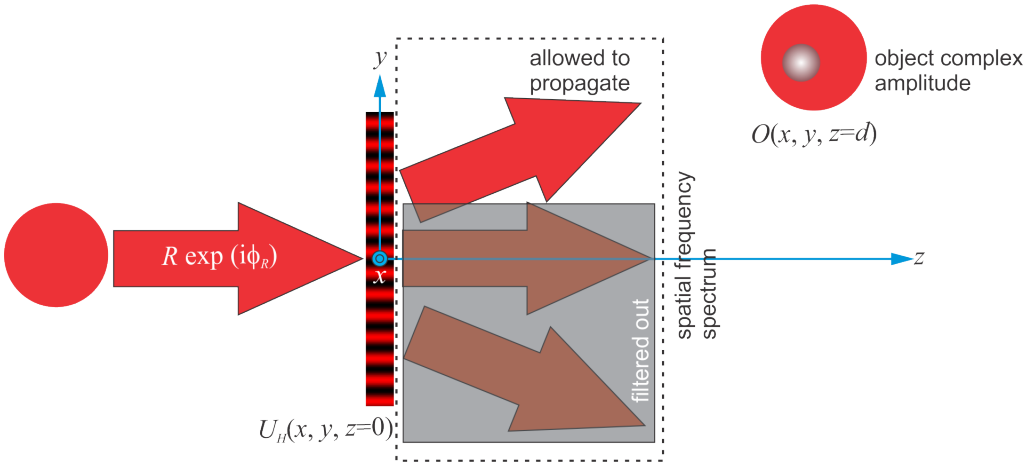

Fig. 3.5: Propagation of the complex amplitude distribution at the hologram

The spatial frequency spectrum or angular spectrum at the hologram plane is just the Fourier transform of the hologram itself (Fig. 3.6). As Eq. (3.4) and Fig. 3.4 and Fig. 3.5 suggests, it contains three distinct terms corresponding to the un-diffracted reference beam, virtual and conjugate object beams (Fig. 3.6b). The spectrum is filtered to retain the frequency information due to object beam alone. The modified spectrum at the hologram plane can be written as [55, 105-106]

$$\bar{U}_H(x,y,z=0) = filt\left[\Im\left\{R\exp(i\phi_R)\,I(x,y,z=0)\right\}\right] = filt\left[\Im\left\{U_H(x,y)\right\}\right] \tag{3.5}$$

This modified spectrum containing object information alone is propagated to the image plane and object information is extracted. It is to be noted here that Eq. (3.5) contains the carrier frequency information. It can be eliminated by shifting the spectrum due to the object (sideband) to the center of the spectral distribution or by recording the carrier fringes (without object) and then subtracting

the corresponding filtered spectrum from the filtered spectrum obtained with the object (carrier plus object).

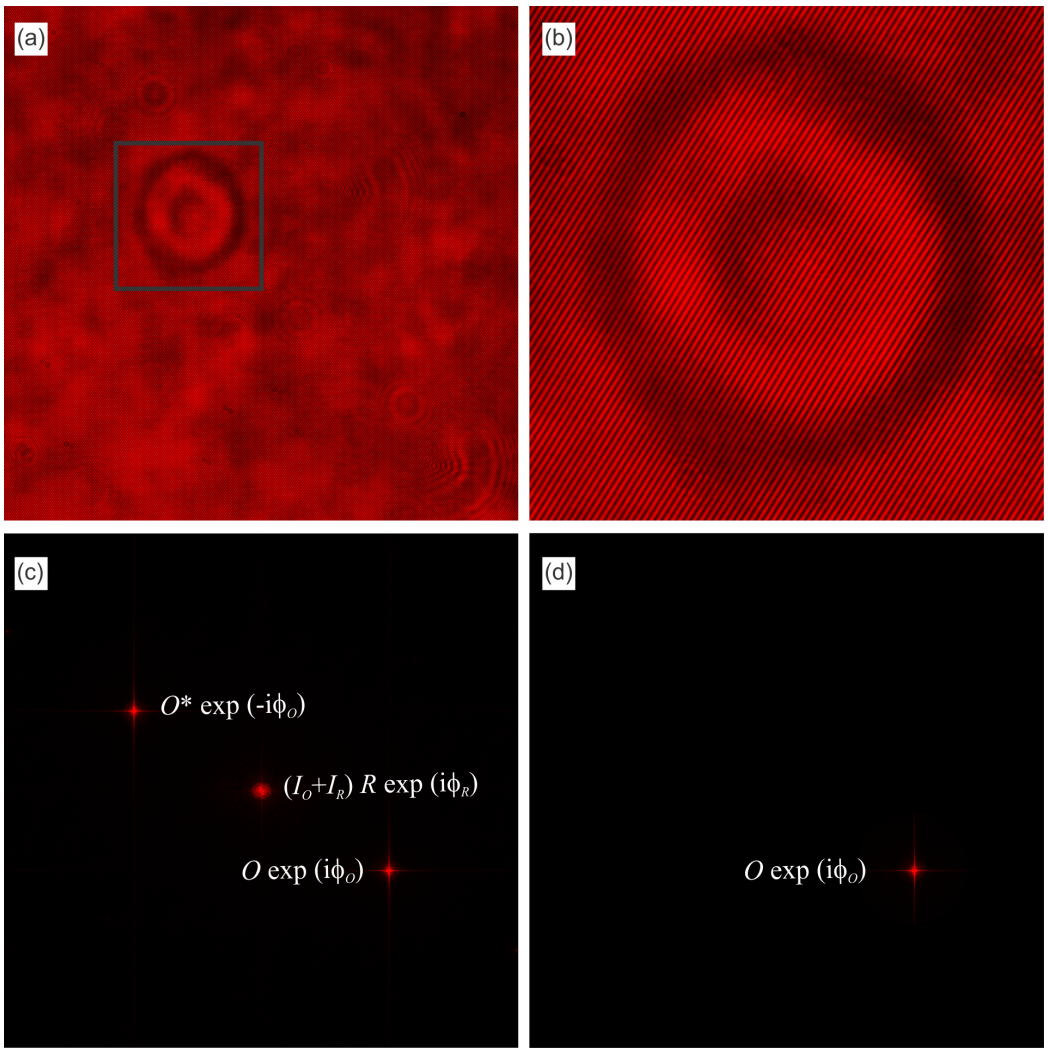

Fig. 3.6: (a) Hologram of red blood cell. (b) Area of interest inside the black rectangle showing fringe modulation due to the object. (c) Spatial frequency spectrum of the hologram illuminated by digital version of the reference beam, showing different diffracted components. (d) Filtered frequency spectrum showing the term corresponding to object and carrier frequency.

The filtered angular spectrum needs to be propagated to the image plane and the object complex amplitude need to be extracted. This requires a propagation function and can be expressed as [105]

$$\hat{U}_O\left(x,y,z=d\right)=filt\left[\Im\left\{U_H\left(x,y,z=0\right)\right\}\right]\exp\left(ik\sqrt{1-\lambda^2 f_X^2-\lambda^2 f_Y^2}\,d\right) \tag{3.6}$$

Exponential term in Eq. (3.6) is the free space propagation function for the filtered angular spectrum, which takes it from z=0 plane to z=d plane, which are parallel to each other and the $\hat{U}(x,$

y, $z=d$) is the spectrum of the object complex amplitude distribution at $z=d$ plane. An inverse Fourier transform is performed on Eq. (3.6) to convert it into spatial domain.

$$U_O(x,y,z=d) = \Im^{-1}\left\{ filt\left[\Im\left\{U_H(x,y,z=0)\right\}\right] \exp\left(ik\sqrt{1-\lambda^2 f_X^2 - \lambda^2 f_Y^2}\, d\right)\right\} \tag{3.7}$$

By changing d in Eq (3.7) the object information at the best focus plane can be obtained. This is called as numerical focusing. This is an added advantage of digital holographic microscopy over conventional microscopy that the object information at different layers can be reconstruct post recording of the hologram without the need for mechanical focusing.

Size of the filter in Eq. (3.7) decides the resolution of the reconstructed images. A filter that can accommodate as much spatial frequencies as possible need to be used to include all the frequency allowed by the imaging lens. But larger filters will let in noise also. This can be reduced using non-linear filters instead of linear filters. In the image reconstructions discussed in this work, Gaussian filters are used for filtering of spatial frequencies.

3.2 Numerical reconstruction of 3D profile of objects

As discussed in the previous section, digital holograms are numerically processed using ASP integral to yield the complex amplitude distribution at the image plane. The intensity of the reconstructed image is obtained from the complex amplitude distribution using

$$I_O(x,y,z=d) = \left|U_O(x,y,z=d)\right|^2 \tag{3.8}$$

One of the biggest advantages of digital holography is numerical focusing. Fig. 3.8 shows the numerical focusing of digital hologram shown in Fig. 3.7a. The figure shows the intensity at different object planes reconstructed from the numerically propagated complex amplitude distribution. For phase objects, whose hologram plane was not at the image plane of the magnifying lens, the best focus plane was found using autofocusing algorithm [107]. Once the position of the best focus plane was determined, it was used in computation of complex amplitude distribution at other time instances also. From Eq. (3.7) it can be deduced that, if the hologram plane is situated at the image plane of the magnifying lens, then the propagation distance d=0, and the whole numerical reconstruction process reduces to Fourier fringe analysis [109]. This makes reconstructions fast and real-time quantitative phase display and analysis a possibility.

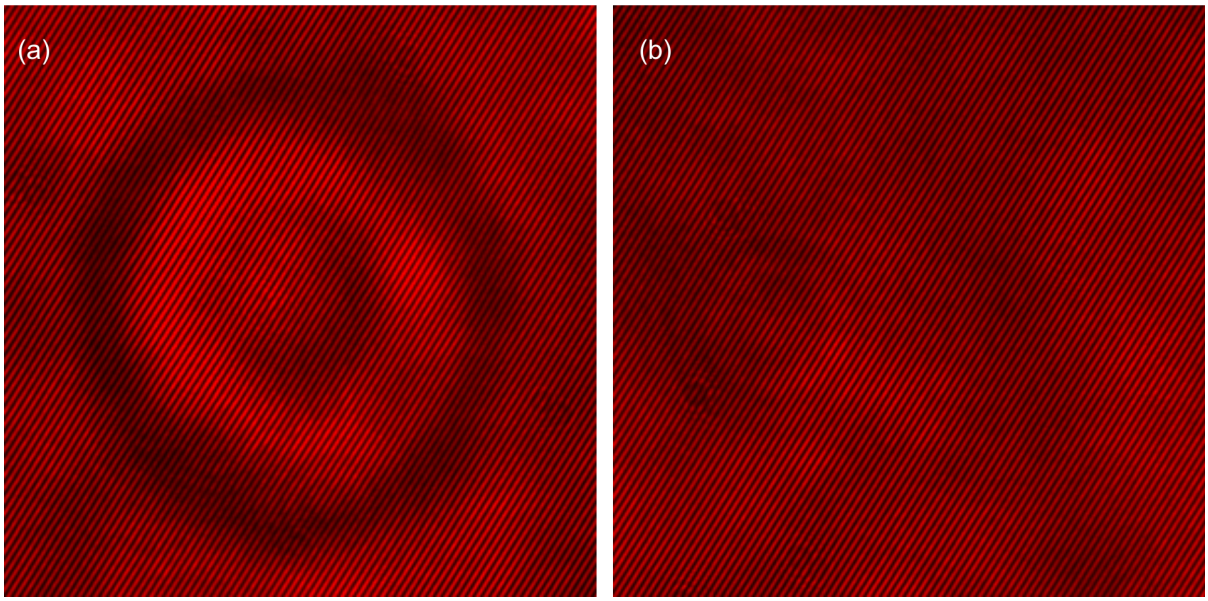

Fig. 3.7: (a) Hologram of a red blood cell. (b) Reference hologram of the same region

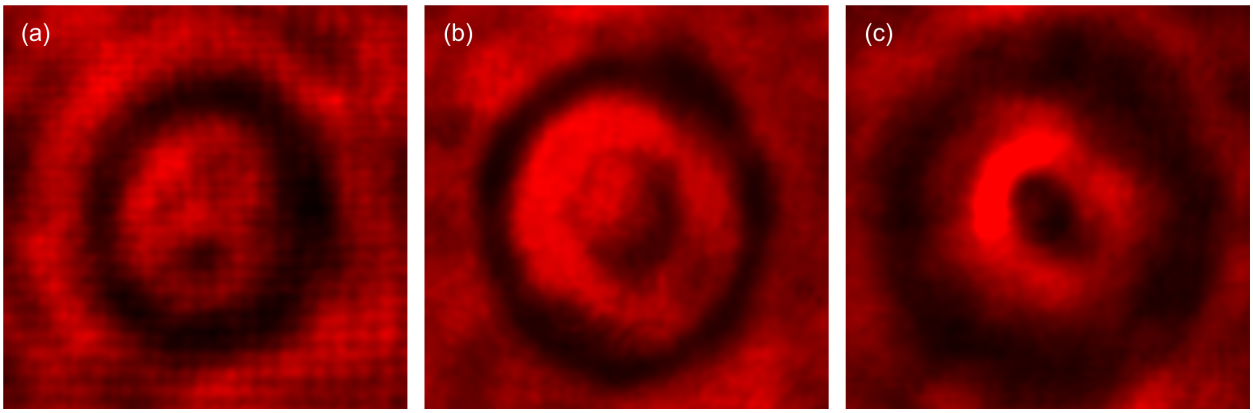

Fig. 3.8: Numerical focusing of digital holograms. (a) Image situated 8μm inside focus. (b) Image at the best focus plane. (c) Image situated 8μm outside focus.

Phase of the object distribution was computed from the angle between the imaginary and real parts of the complex amplitude distribution and is given by

$$\phi_O(x,y) = \tan^{-1}\left[\frac{\mathrm{Im}(U_O)}{\mathrm{Re}(U_O)}\right] \tag{3.8}$$

where 'Im' and 'Re' represents the Imaginary and Real part of the complex amplitude distribution. To eliminate the phase due to aberrations in the optical system, bringing out the phase due to the object alone a reference hologram (Fig. 3.7b), which in its field of view contains the medium

surrounding the object was also recorded, numerically processed and phase extracted (ϕ_R). The phase difference ($\Delta\phi=\phi_O-\phi_R$) is related to the object thickness through [55]

$$\Delta\phi(x,y)=\phi_O-\phi_R=\frac{2\pi}{\lambda}(n_O-n_R)h(x,y) \tag{3.9}$$

where n_O and n_R are the constant average refractive indices of the object and the medium surrounding it respectively. Fig. 3.9a shows the phase difference profile using the holograms shown in Fig. 3.8. Thickness profile of the object (red blood cell for the hologram in 3.7a) was computed by using n_O=1.42 for the cell and n_R=1.34 for blood plasma (medium surrounding the cell) [130] and is shown in Fig 3.8b.

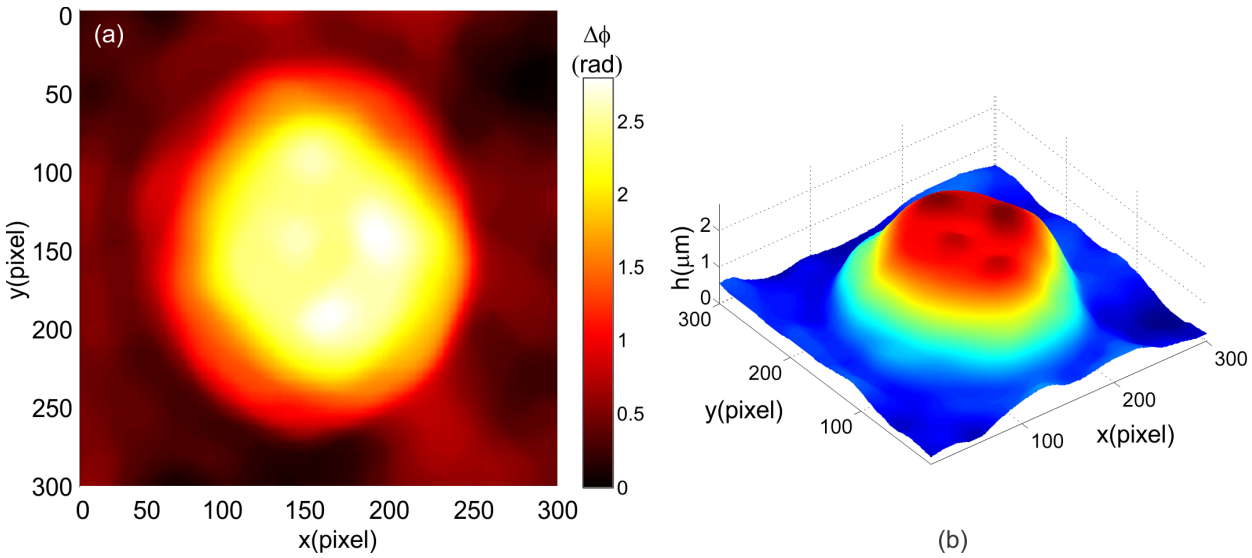

Fig. 3.9: (a) Phase difference between object and reference holograms. (c) Thickness profile of the object after plugging in the refractive index values in Eq. (3.9).

3.3 Digital holographic interference microscopy

The easiest way to construct a Digital Holographic Interference Microscope (DHIM) is to use the Gabor recording setup [14] with no lenses for imaging [16, 18, 20-22]. It is usually implemented by illuminating a sparse object distribution by an expanding spherical wavefront from a point source. The portions of the wavefront unscattered by the object acts as the reference. From Fig. 3.3 an Eq. (3.4), it can be seen that, the biggest drawback of Gabor geometry is that during reconstructions, the three diffracted components overlap, obscuring each other. Extraction of phase information from such a hologram requires some apriori knowledge of the object distribution. The

reconstructions are also computationally exhaustive [21-22]. Use of a lens in Gabor setup can increase the magnification and resolution [23-24], but the phase extraction will still remain an issue. A separate reference beam can be used in the Gabor configuration by the use of a beasmpsiltter leading to in-line setup [25-33]. Use of a separate reference beam makes it possible to image denser object distributions, but here also the phase cannot be computed without an ambiguity from a single hologram. Use of a phase-stepping mechanism can provide the exact object phase in in-line geometry, but requires a series of holograms, and cannot be termed as single shot technique [108]. The easiest way to extract phase information from a single hologram is to spatially separate the virtual object, conjugate object and undiffracted reference beams. This requires an off-axis setup, first proposed by Leith and Upatnieks [108], where the object and reference beams superpose at an angle (Fig. 3.10). Since the three beams will be separated spatially, a single hologram will provide complete object phase information, leading to a single-shot technique.

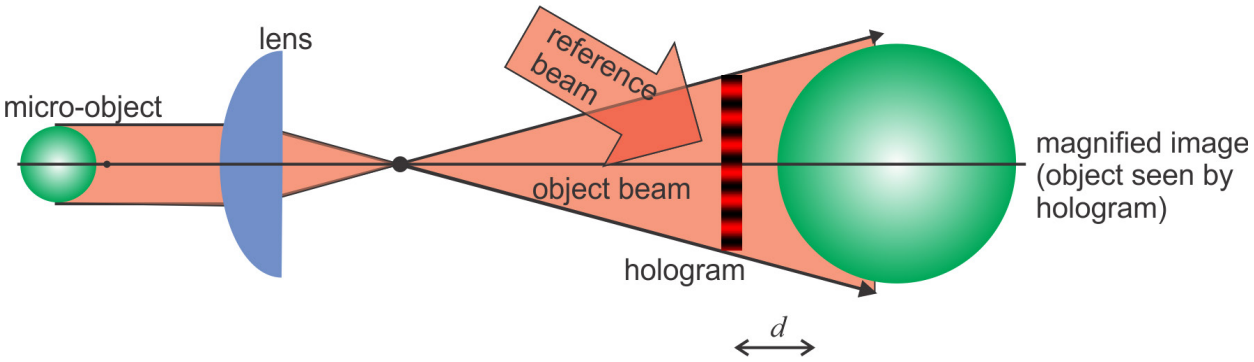

Fig. 3.10: Concept of off-axis digital holographic microscope

The simplest off-axis holographic microscope (Fig. 3.10) will have a single lens to magnify the object. A digital sensor is kept in the path of the magnified object beam, but not necessarily at the image plane of the magnifying lens. At the sensor the object beam is superposed with an off-axis reference beam forming the hologram. For the digital sensor, magnified image of the object formed by the lens will act as the new object situated at a distance d from the hologram plane, where d is the distance between the magnified image and the digital array. It is also the distance, the complex amplitude distribution at the hologram, obtained by illuminating the hologram by the digital replica of the reference beam, needs to be propagated to obtain the best focus image due to the magnifying lens.

3.4 Two-beam DHIM based on Mach-Zehnder interferometer (MZ-DHIM)

For transmission mode interference microscopy, geometry based on Mach-Zehnder interferometer (Fig. 3.11) is the most widely used configuration [34-76]. It has the advantage of automatic path length adjustment and almost equal beam ratios (for phase objects) leading to high contrast fringes, whose fringe density is adjustable.

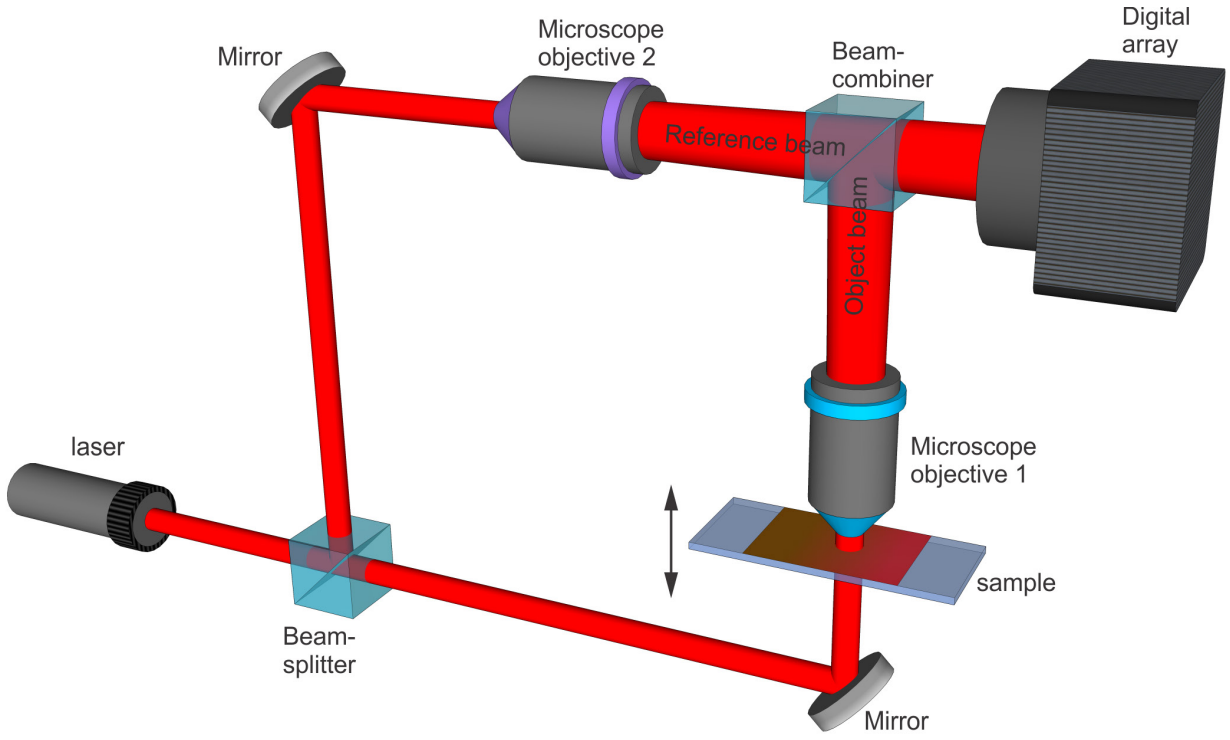

Fig. 3.11: Transmission mode two-beam off-axis Mach-Zehnder interferometer based Digital Holographic Interference Microscope for 3D imaging of phase micro-objects.

Fig. 3.11 shows the basic configuration of two-beam DHIM based on Mach-Zehnder configuration. Beam from a laser source is split into two (50:50) by a beamsplitter. One of these beams trans-illuminates the sample under investigation. Object is then magnified by a microscope objective of appropriate magnification and numerical aperture. This beam will act as the object beam. The other beam is also passes through a microscope objective of similar configuration to make sure that the curvatures of the two wavefronst match at the sensor plane. This will lead to creation of linear fringe system, which will result in a frequency spectrum easier to analyze. A curved fringe system will result in a spectrum that is spread, which may result in the sidebands overlapping with the DC term, where as a linear fringe system will result in a spectrum that has

very sharp sidebands, thereby reducing this overlapping. The beams are then superposed using an second beamsplitter, which can be called as a beam-combiner. The superposed beams lead to creation of holograms at the sensor plane.

3.5 Three-dimensional imaging of red blood cells using MZ-DHIM

Fig. 3.12a shows the hologram of a red blood cells recorded using a 100×, NA=1.25 commercial grade microscope objective lens operated in dry mode and a CCD array (8-bit dynamic range, 4.65μm pixel pitch), placed at the image plane of the magnifying lens. A He-Ne laser working at a vacuum wavelength of 611nm with maximum output power of less than 2mW was used as the light source. Thin blood smears on microscope slides covered with cover slides were used as the object. Fig. 3.12c shows the reference hologram for the same set of cells, recorded from the same slide, from a region which only had blood plasma.

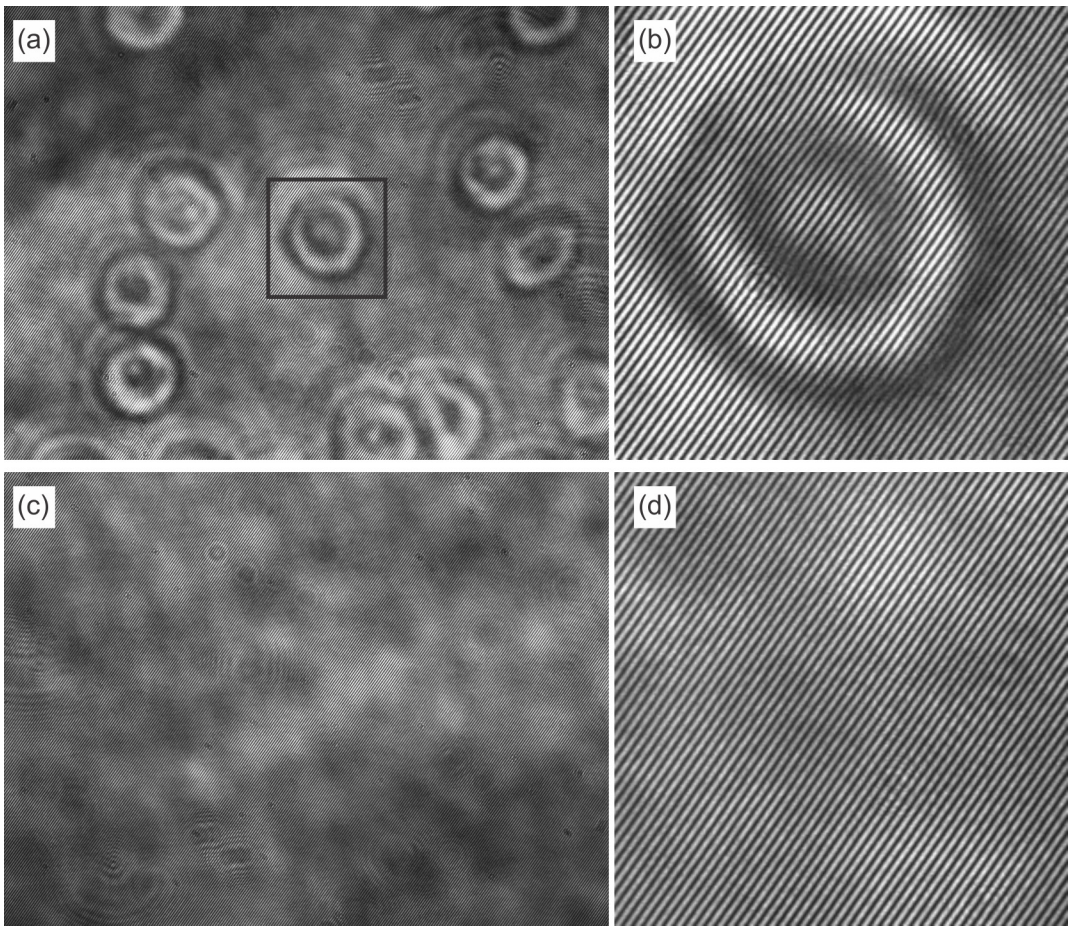

Fig. 3.12: (a) Hologram of red blood cell distribution in thin blood smears. (b) Reference hologram for the same set of cells.

Recorded holograms were numerically reconstructed using ASP integral explained in Section 3.1 and the phase of object holograms (fig. 3.13a) and reference holograms (Fig. 3.13b) were extracted. Phase subtraction ($\Delta\phi$) brings out the object information (Fig. 3.13c) after nullifying the phase due to the aberrations, which remained same between the exposures. As explained in the previous section this phase difference distribution is then used in Eq. (3.9) along with constant average refractive index value of 1.42 for red blood cells and 1.34 for blood plasma [130] to reconstruct the thickness profile of red blood cells (Fig.3.13d).

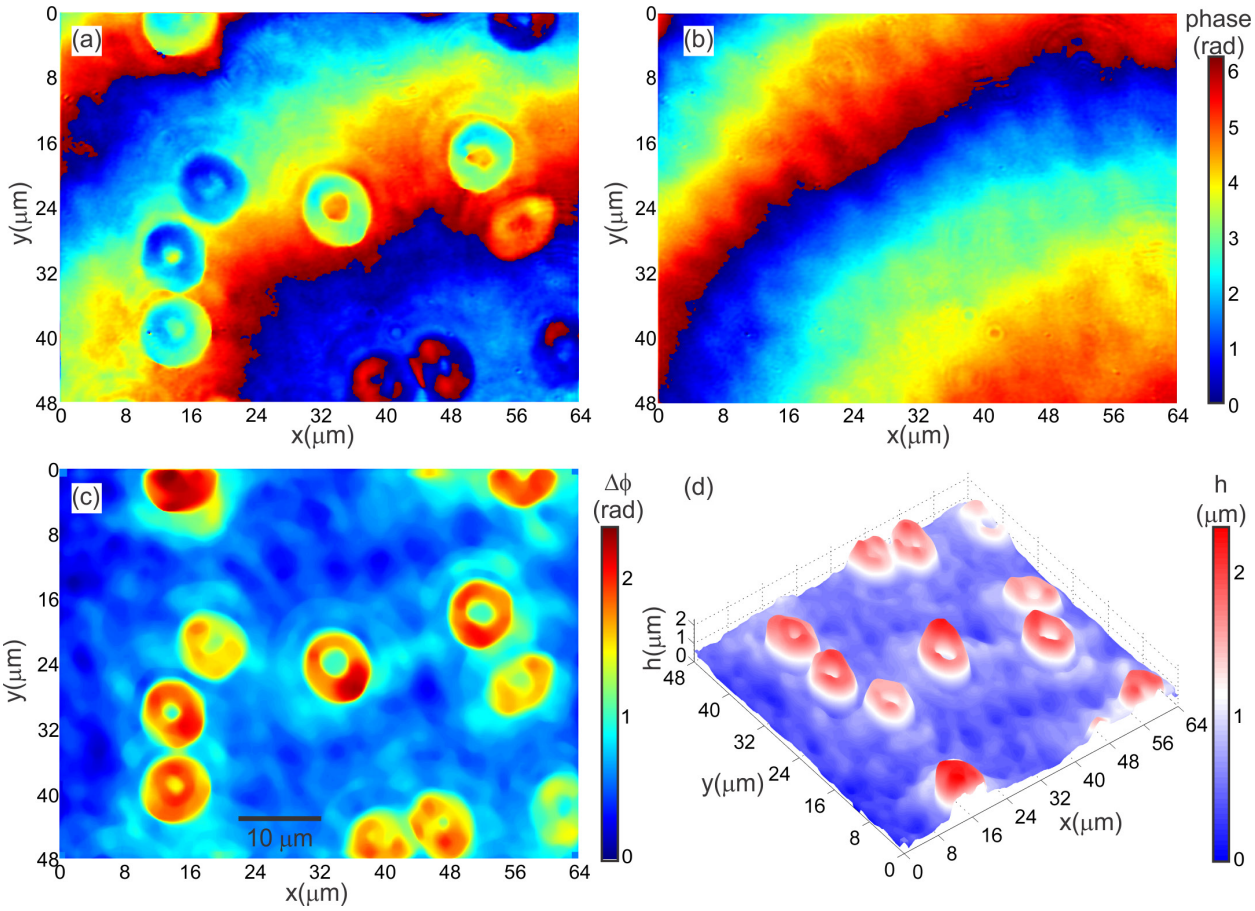

Fig. 3.13: Thickness computation of red blood cells. (a) Phase distribution of object hologram. (b) Phase distribution of reference hologram. (c) Phase difference obtained by subtracting reference phase from object phase. (d) Cell thickness distribution obtained by using the phase difference distribution in Eq. (3.9) along with the refractive index values of the cell and the surrounding medium.

For automatic cell location identification and thickness extraction of individual cells, the background phase difference distribution in Fig. 3.14a need to be reduced. It was achieved by thresholding the phase difference distribution by the mean of the background phase variation. Further, cells attached to each other were eliminated by computing the eccentricity of the projected

area. Also, the cells at the boundary were also removed from the phase map. The phase map after noise reduction and elimination of boundary cells and connected cells is shown in Fig. 3.14b. The region of the identified cells is shown in Fig. 3.14c and three-dimensional thickness distribution of the identified cells is shown in Fig. 3.14d.

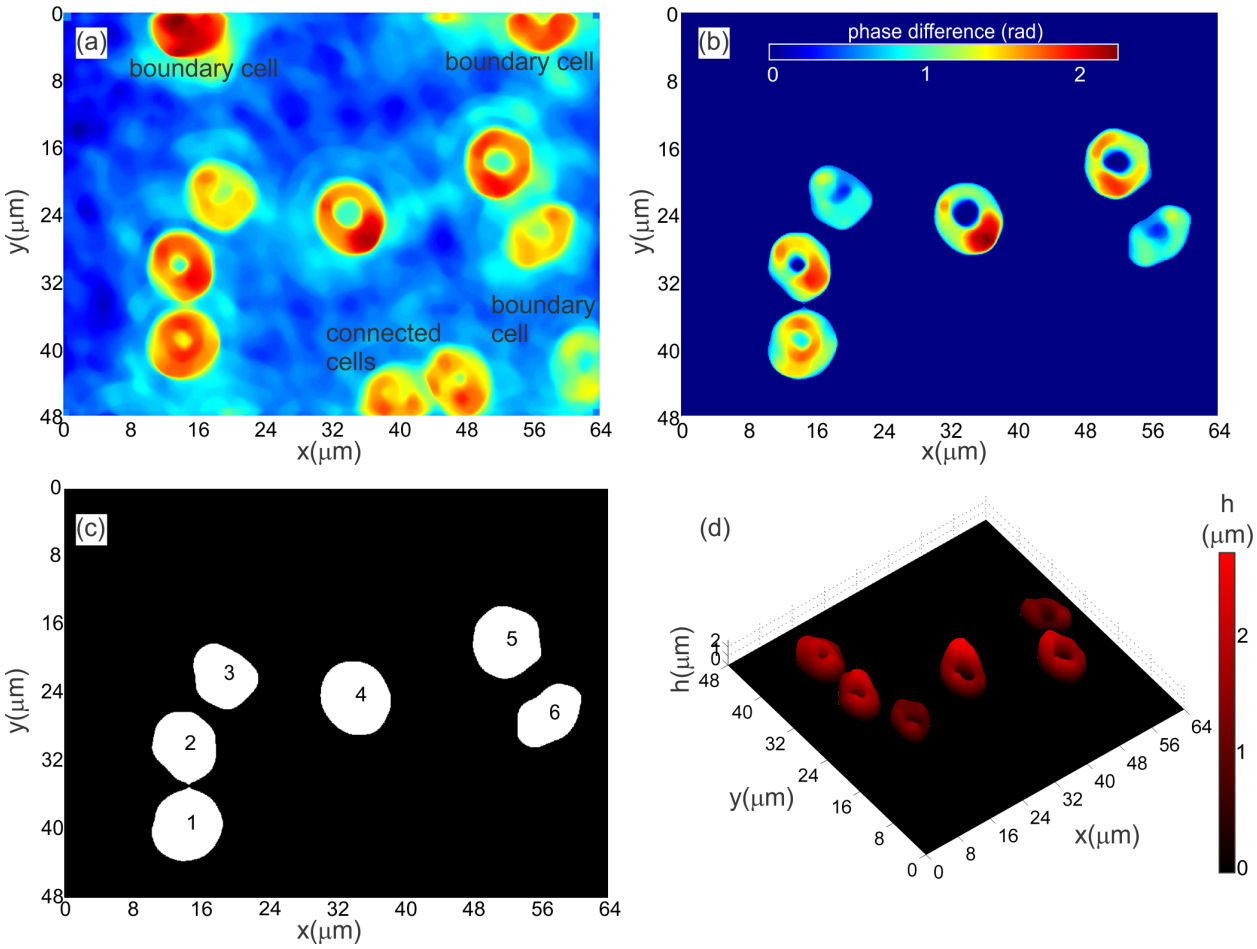

Fig. 3.14: Cleaning of phase maps and identification of cell locations. (a) Cells at the boundary and connected cells. (b) Phase map after thresholding and removal of boundary as well as connected cells. (c) Identified cells and cell locations. (d) Thickness distribution of identified cells.

Using digital holographic microscope, multitude of cell parameters based on the morphology (thickness distribution) of the identified cells can be extracted. These parameters can be classified into three i) physical parameters based on the output from a single hologram, ii) mechanical parameters based on the output from a time series of holograms and iii) optical parameters. These parameters are enumerated in Table 3.1. These parameters can provide important information on the state of health of the cells and can act as discriminators for cells. These parameters were investigated to see, whether it can be used to characterize, compare and identify cells, leading to automatic disease identification

Table 3.1: Blood cell parameters obtained using digital holographic microscope

	Parameters
Physical parameters (from a single hologram of the cells)	1) Thickness (Mean, maximum, minimum, width, Coefficient of variation) 2) Dry mass 3) Projected area 4) Volume 5) Curved Surface Area 6) Total Surface Area 7) Surface Area to Volume Ratio 8) Surface Area to dry mass ratio 9) Projected area to volume ratio 10) Sphericity index 11) Eccentricity 12) Circularity 13) Shape 14) Thickness variance 15) Thickness Kurtosis 16) Thickness skewness
Mechanical parameters (from a time series of holograms).	1) Amplitude of cell fluctuation 2) Cell volume fluctuation 3) Frequency of cell fluctuation 4) Cell motility 5) Dynamic light scattering 6) Sub-domains
Optical parameters (from a series of holograms with different projection angles of source laser beam - tomography)	1) Absorption 2) Refractive index 3) Refractive index variation

3.6 Label-free identification of malaria using MZ-DHIM

Malaria is still one of the most widespread and potentially fatal diseases especially in developing nations. Proper medication and cure of malaria depends upon its identification. Optical microscopy is still the best tool for malaria identification [131]. Collected blood samples, suspected of having malaria parasites, are chemically treated initially (with Giemsa stain) [129, 132]. The stain gets attached to red blood cells infected by the parasite, changing its absorption profile compared to

normal red blood cells. A blood smear is then made on a microscope slide and a trained technician observes these under a microscope and identifies cells with altered absorption profile. But identification visual inspection depends upon the quality of the labelling agent, microscope as well as on the expertise of the microscopist. So, a device, which can automatically differentiate (without the need of a trained professional) between normal and infected red blood cells will greatly benefit health care professionals. If the device is compact, it will have the added advantage of field portability, thereby enabling remote malaria identification and will be useful in areas that cannot be easily accessed.

When malaria infected mosquito bites a person, the transmitted parasites invades the liver and multiplies before affecting the RBCs in the blood stream. The symptoms of the fever may not be visible before a week or up to a month after infection. When malaria parasites affect RBCs, significant changes in cell volume and morphology occurs over the course of parasite infection. At trophozoite stage of infection, it has been reported that the cell volume increases by about 17%, followed by reduction in cell volume by up to 22% at the schizont stage [132]. So, the morphology of red blood cells changes when malaria parasites infect them. DHIM is a tool for label free quantitative imaging of cells. It provides several cell parameters based on cell morphology, that is usually obtained using a hematology analyzer. It will be interesting in using DHIM technique for studying morphological changes and identification of malaria infected RBCs without the aid of staining reagents.

For imaging with MZ-DHIM, healthy and malaria tested positive (severe malaria) samples were obtained from pathology lab. The samples were centrifuged to obtain the red blood cells. A thin smear of the red blood cells was made on a microscope slide and imaged using the MZ-DHIM. Holograms of both healthy and malaria infected samples were recorded and reconstructed numerically to obtain the phase distributions. The phase distributions were then converted into cell thickness distributions. Fig. 3.15 shows the three-dimensional thickness distribution as well as the cross-sectional thickness distribution for 6 healthy red blood cells and Fig. 3.16 shows the same for malaria infected red blood cells. A comparison between the two figures shows that the shape of red blood cells changes from its normal doughnut shape (Fig. 3.15) when infected by malaria (Fig. 3.16). It can also be seen that cells in the malaria infected samples have larger volume compared to healthy samples [63, 72-73].

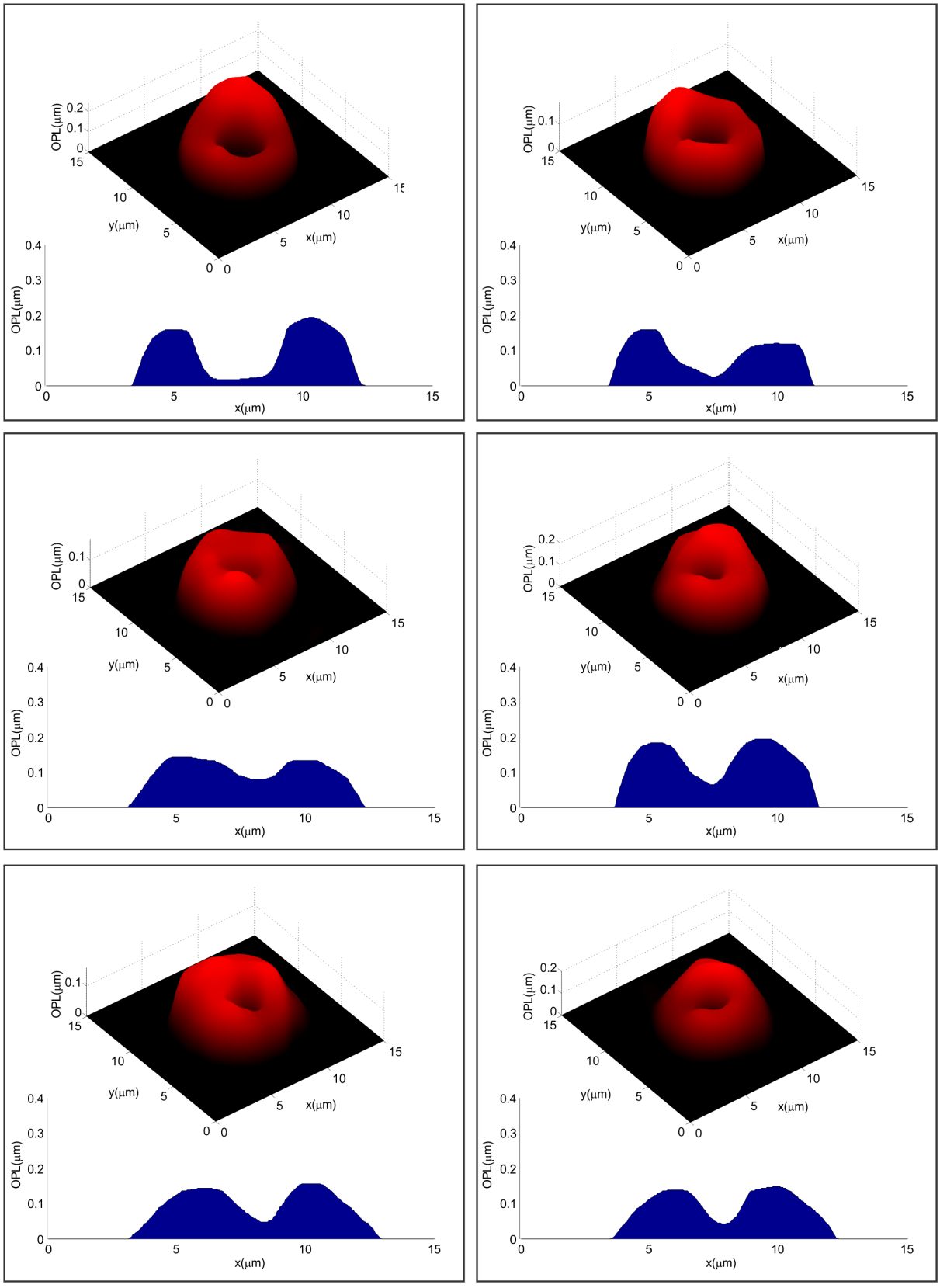

Fig. 3.15: Obtained thickness distribution and cross-sectional thickness profile of healthy red blood cells

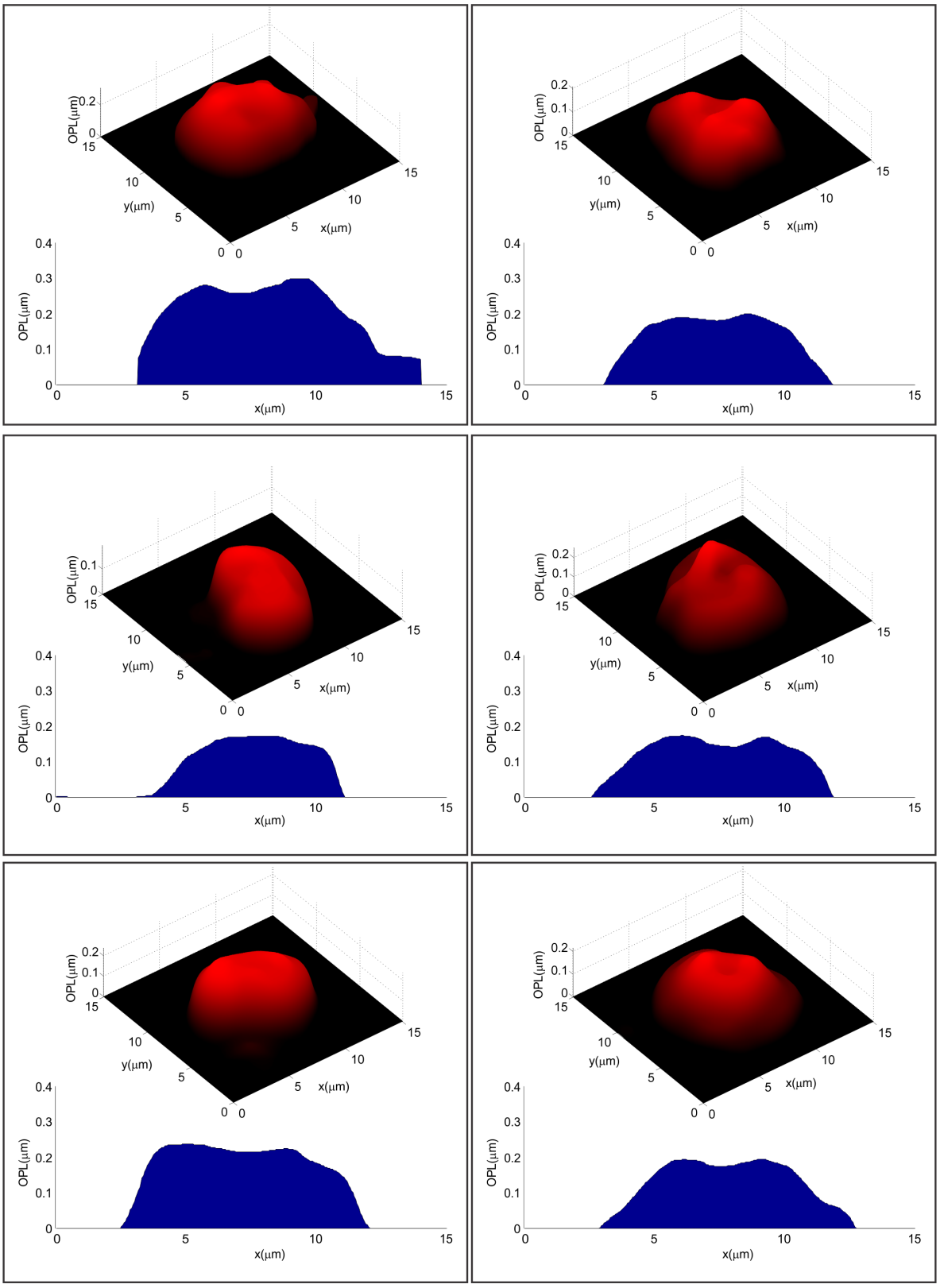

Fig. 3.16: Obtained thickness distribution and cross-sectional thickness profile of red blood cells in malaria tested positive sample.

In the studies conducted, Optical Path Length (OPL) profile of the cells, which represents the product of cell thickness and the cell refractive index was used to extract cell parameters, which depends upon the cell morphology. Use of OPL makes the computation more accurate since, the assumption of a constant average refractive index may turn out to be wrong, especially for cells affected by diseases. Mean OPL was computed by averaging the OPL over the identified cell location and region (Fig. 3.14c) using.

$$OPL_{mean} = \frac{1}{M \times N} \sum_{i=1}^{M} \sum_{k=1}^{N} OPL(i,k) \tag{3.10}$$

where $OPL(i,k)$ is the OPL value at the $(i,k)^{th}$ pixel of the optical path length distribution map and M and N are the total number of pixels in a row and a column respectively of the OPL array. Mean of the OPL is a measure of many cell parameters including the dry mass (max excluding water) of the cell [65]. Maximum, minimum as well as the standard deviation and coefficient of variation (CV=standard deviation/mean) of the OPL distribution were also computed. Fig. 3.17a shows the mean OPL values computed for healthy and malaria infected samples. Fig. 3.17b shows the probability distribution of the OPL_{mean} distribution. Parameters obtained from 52 healthy cells and 47 malaria infected cells were used in the calculations.

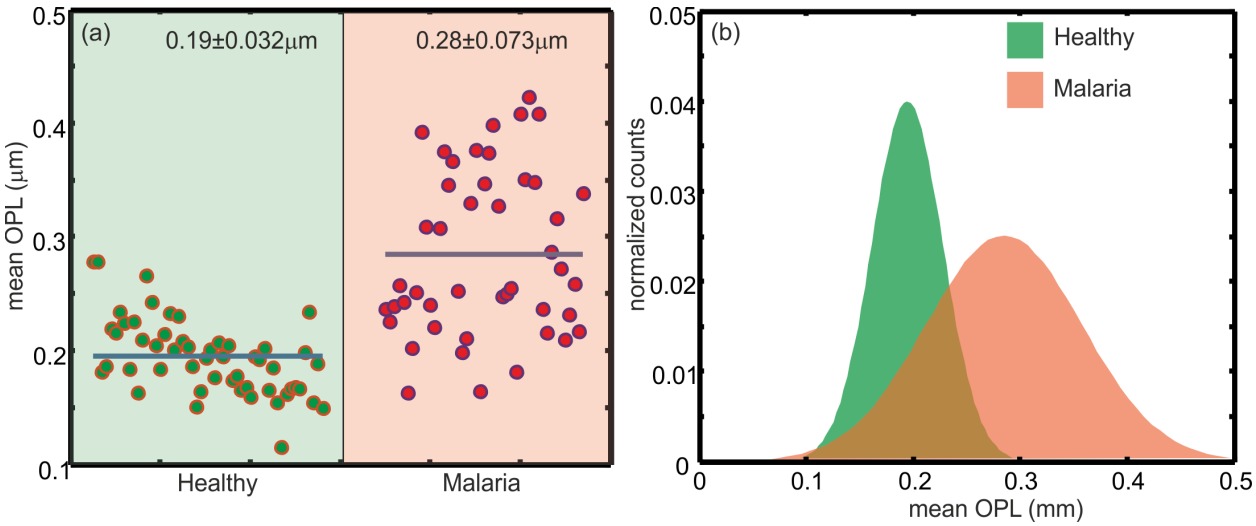

Fig. 3.17: Mean optical thickness of cells measured form the OPL profile. (a) Values obtained for individual cells. (b) Probability distribution. The straight line in Fig. 3.17a indicates the mean value.

The mean thickness of malaria infected cells are more, which was expected since the presence of the malaria parasite inside the cell increases the OPL of light propagating through the cells. Table 3.2 shows the mean value as well as standard deviation of extracted cell parameters [76].

Projected area (A_{proj}) of the cell is calculated from the number of pixels occupied by the cell on a flat surface (N_{pix}) and by knowing the pixel size of the sensor and the magnification of the lens.

$$A_{proj} = \frac{\Delta_{pix}^2}{M_L^2} N_{pix} \tag{3.11}$$

where Δ_{pix} is the size of the camera pixel, M_L is lateral magnification of the optical system. Diameter is directly computed from the projected area by considering it as circular in shape. One of the other parameters of interest that can be computed from projected area is eccentricity of the cells. Eccentricity represents the amount of deviation of the shape of the projected area from circular shape. This also is a measure represents a change in the shape (on a flat surface) of the cells. Eccentricity is given by

$$e = \frac{r_{\max} - r_{\min}}{r_{\max} + r_{\min}} \tag{3.12}$$

Optical surface area of the cells is the summation of the projected area and the curved surface area and is given by

$$SA = dA \sum_{i=1}^{M} \sum_{k=1}^{N} \sqrt{\left(1 + \delta h_x^2\left(i,k\right) + \delta h_y^2\left(i,k\right)\right)} + A_{proj} \tag{3.13}$$

In the above equation dA is the area occupied by each pixel, considering the lateral magnification of the system, δh_x and δh_y are the gradients of thickness along the x and y directions of the cell thickness profile and i and k are the position of the pixel in the region where the cell existed [65]. Surface area is important from the point of view of oxygen carrying capacity of red blood cells. Larger surface area leads to larger probability of oxygen permeation into the cells.

Optical volume was also computed from the OPL distribution and the area of each pixel in the distribution map (dA) through.

$$Vol = dA \sum_{i=1}^{N} OPL_i \tag{3.14}$$

where N is the total number of pixels occupied by a cell. Surface area to volume ratio is a very important parameter, which provides insight into the oxygen carrying capacity of the cell as well

as its shape (flat or spherical). Fig. 3.18 shows the surface area to volume ratio of individual cells along with the probability distribution.

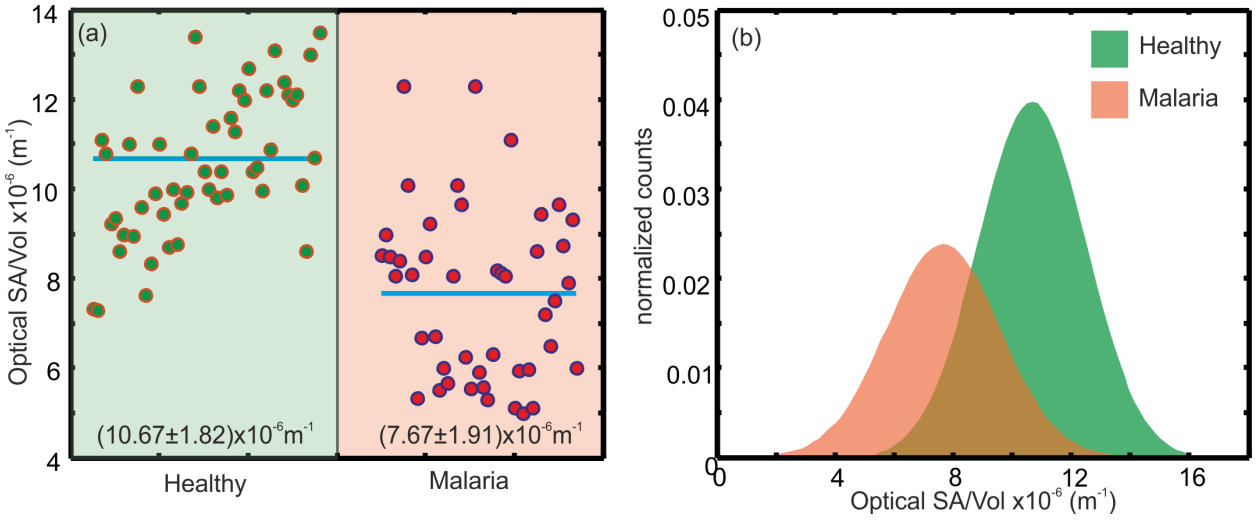

Fig. 3.18: Surface area to volume ratio. (a) Values for individual cells. (b) Probability distribution

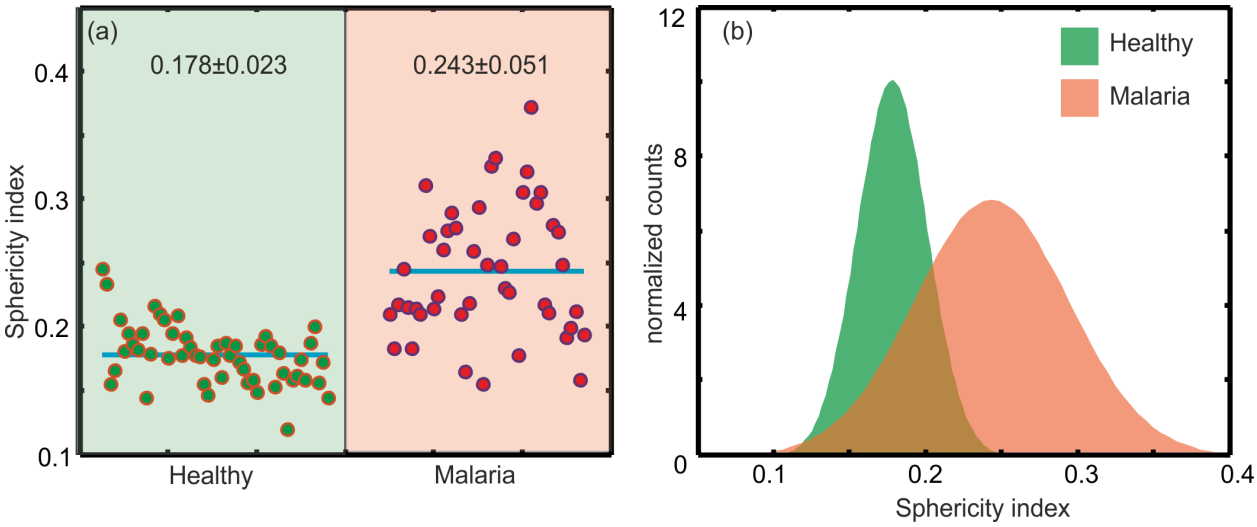

Fig. 3.19: Sphericity value. (a) Values for individual cells. (b) Probability distribution

Surface to volume ratio also indicate a deviation from the doughnut shape in the case of malaria infected cells. Sphericity index quantifies the shape of the cell in terms of a sphere (roundness of the cell). For a perfectly spherical it should be 1. It is given by

$$S = \frac{\pi^{1/3}(6Vol)^{2/3}}{SA} \tag{3.15}$$

Fig. 3.19 shows the obtained sphericity values for red blood cells from healthy and malaria tested positive samples. It indicates that the malaria infected red blood cells are more round and have more volume [109].

Table 3.2: Physical parameters of Red Blood Cells [76]

Parameter	Healthy sample	Malaria tested positive sample
Diameter (µm)	7.62±0.54	7.31±1.37
Mean OPL (µm)	0.19±0.032	0.28±0.073
Optical Volume (fL)	17.89±3.41	21.75±9.84
Projected Area $\times 10^{12}$ m^2	46.04±6.48	43.87±17.07
Surface Area by Volume ratio $\times 10^{6}$ m^{-1}	10.67±1.82	7.67±1.91

Individually, the parameters given in Table 3.2 may not be able to discriminate between healthy and malaria infected cells. A correlation between the parameters will provide a better insight into the state of health of the cells. For example, Fig. 30 shows the correlation map between optical volume and optical surface area to volume ratio, where a nice bunching of the cells can be observed

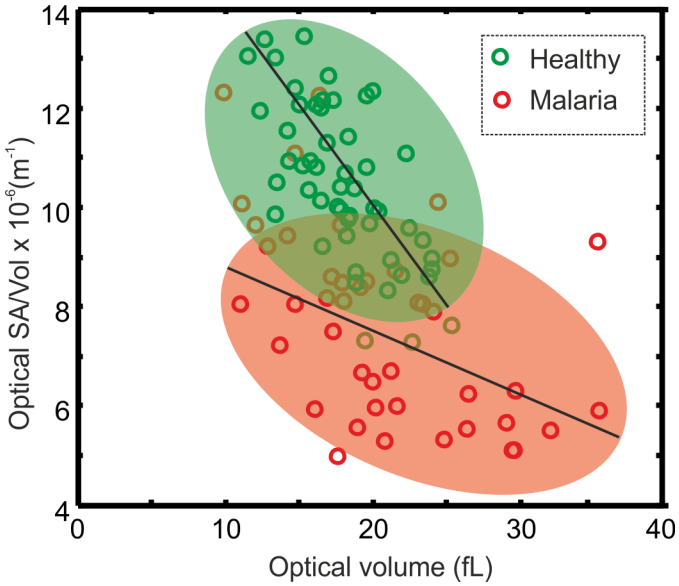

Fig. 3.20: Correlation map between optical volume and optical surface area to volume ratio.

One of the interesting things that can be observed from Table 3.2 is that all the extracted parameters indicate that the malaria infected cells have different spatially varying OPL distribution (shape) compared to healthy cells. So the shape of the cell may be used to discriminate between the cells. Databases of OPL distribution (shape) of healthy red blood cells and malaria infected red blood cells were created. Shape of an individual healthy cell was compared with all the other cells in the data base of healthy cells and a cross-correlation coefficient (computed using Pearson product-moment correlation), which is the average of all these values was obtained (Fig. 3.21). This is repeated for all the healthy cells in the database. The same procedure was repeated to find an average of cross-correlation coefficient [63] between the shapes of each malaria infected red blood cell and all the healthy red blood cells. Here also the cross-correlation coefficient for all the cells in the database of malaria infected cells were computed. The correlation coefficient between the shapes of two cells is given by

$$r_{XY} = \frac{1}{\sigma_X \sigma_Y (N-1)} \sum_{i=1}^{N} (X_i - \bar{X})(Y_i - \bar{Y}) \tag{3.16}$$

where $\bar{X}$ and $\bar{Y}$ are the sample means of X and Y and σ_X and σ_Y are their standard deviations. In the case of cells X and Y represents the OPL distribution of a particular cell. To improve the possibility of correct identification OPL distribution obtained from different object layers by numerical focusing were used (Fig. 3.21) in the computation. The effect of numerical focusing on the OPL distribution in the case of healthy and malaria infected red blood cells are shown in Fig. 3.22 [63, 73]. In the case of multiple planes, correlation value for each individual plane for a particular cell pair was calculated using Eq. (3.16) and then averaged.

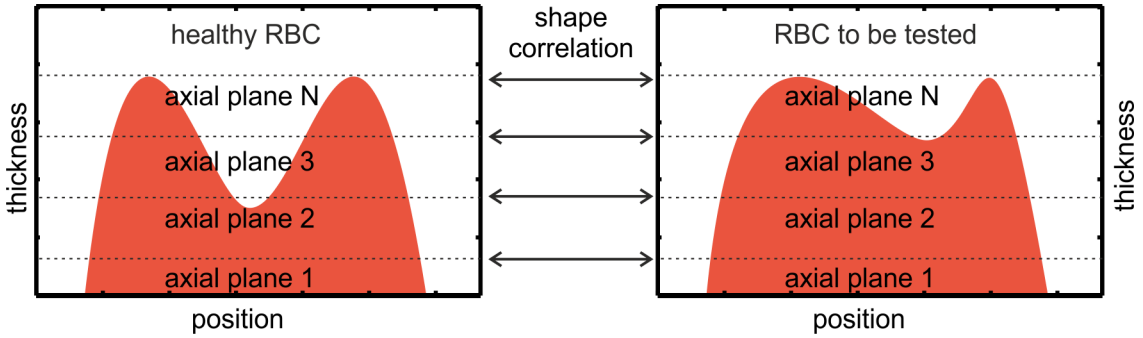

Fig. 3.21: Automatic cell identification by shape comparison. Reconstructed OPL distribution from 20 layers (N=20) were used for identification of cells.

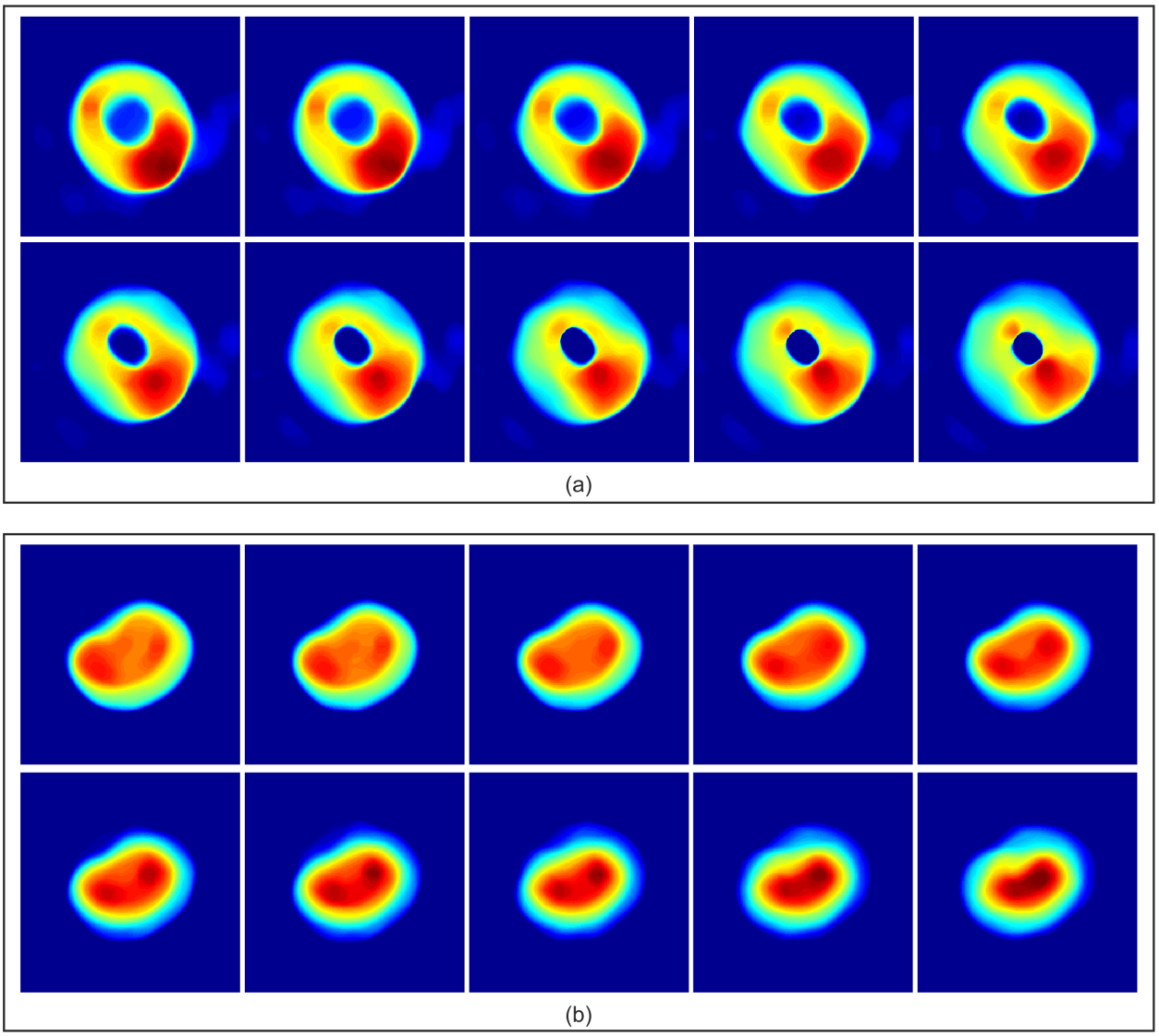

Fig. 3.22: Quantitative phase images of red blood cells at 10 axial planes separated by 0.24μm. (a) For healthy cells. (b) For malaria infected cells.

In the computation of cross-correlation values, data from 20 axial planes separated by 0.12μm were used. Fig. 3.23a shows the obtained shape correlation values by comparing healthy cells with healthy cells (H-H correlation shown by green dots) and healthy cells with malaria infected cells (H-M correlation shown by red dots). The mean value of shape cross correlation values is shown as straight lines in the plot. The average of the mean value of H-H shape correlation and H-M shape correlation, shown by black straight line in Fig. 3.23a acted as the discriminator. Fig. 3.23b shows the distribution plots for the shape correlation values. From Fig. 3.23 it can be seen that the shape correlation value acts a cell discriminator.

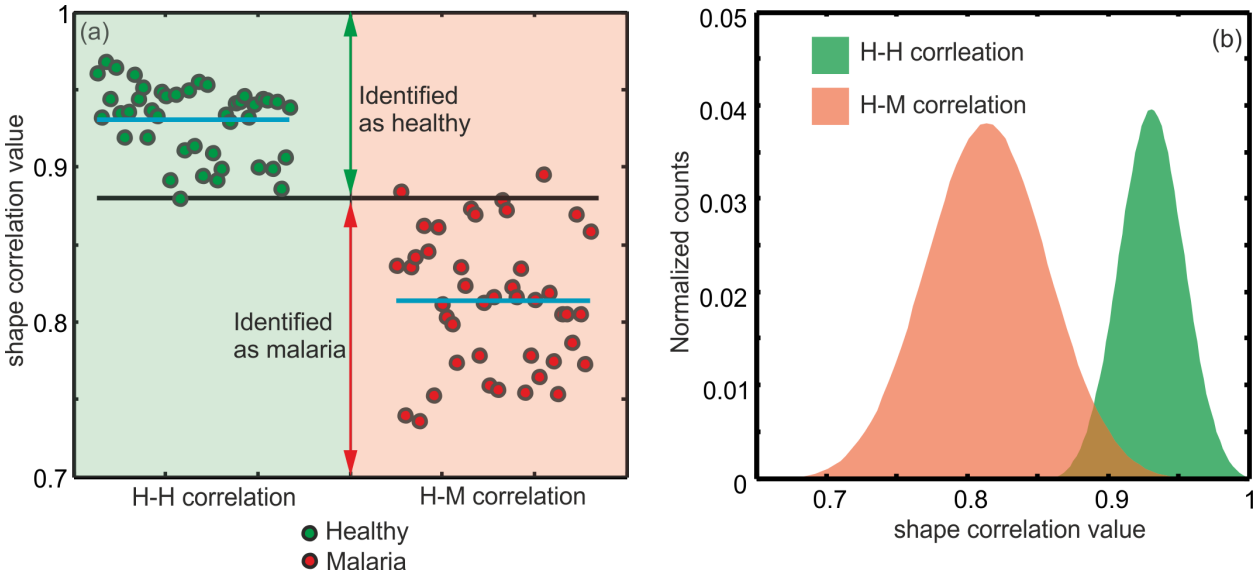

Fig. 3.23: Automatic, label free identification of malaria infected red blood cells using shape correlation values. (a) Computed shape correlation values for individual cell pairs. (b) Distribution plot of shape correlation values. Straight black line in Fig. 3.23a act as the cell discriminator shape correlation value.

Using the shape correlation value obtained from multiple axial planes of the cells, true positive rate (TPR) of cell identification was better than 95% and the false positive rate (FPR) was less than 3%.

3.7 Device

A quantitative phase microscope based on the Mach-Zehnder interference configuration was devised by 3D printing the support structure of the microscope (Fig .3.24). The optical elements were incorporated into the device. Laser source was externally coupled to the microscope and used to trans-illuminate the sample under investigation. The advantage of coupling the laser externally to the microscope is that without disturbing the microscope, various types of lasers and wavelengths could be used to investigate the sample. The microscope comprised of a 3D printed structure. The microscope was fabricated in a modular format so that the optical components can be easily introduced into the microscope structure. Beamsplitters, mirrors and microscope objective lenses were then placed at their appropriate positions as shown in Fig. 3.24. The holograms were recorded using an 8-bit CCD array with 4.65mm pixel pitch was used for recording of the holograms. The holograms were processed by the technique presented in the previous sections of this chapter.

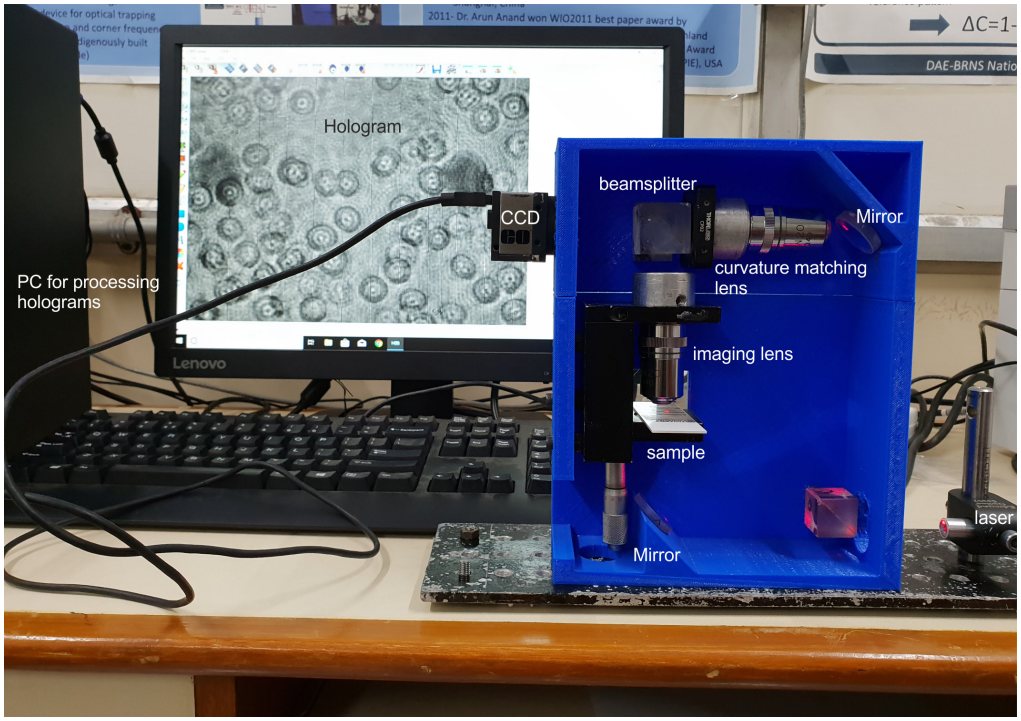

Fig. 3.24: Clinical version of the two-beam DHIM employing Mach-Zehnder interferometer geometry

3.8 Conclusions

Mach-Zehnder DHIM, even though requires many optical elements to construct, provides accurate 3D thickness distributions of cells. It has shown the potential of DHIM devices in quantifying cells and extraction of cell parameters for their characterization, comparison and identification. Integration of DHIM (for three-dimensional imaging of RBCs) and shape correlation algorithms applied to the OPL distribution has the potential to be an automatic method to discriminate between different classes of RBCs. Comparison of the shape of the test cell with the database of healthy and infected cells may indicate whether the cell is healthy or not. A database of parameters for cells identified with different diseases can be created. By comparing the extracted cell parameters based on cell morphology with the parameters of already identified cells, will lead to automatic disease identification. From the results it can be seen that DHIM can provide a multitude of blood cell parameters based on its morphology, usually provides by hematology analyzer. This aspect of the microscope can be exploited to convert it into a blood cell analyzing unit. The main drawback of the two-beam MZ-DHIM is its bulkiness, which prevents it from being converted into a field portable device. But the prototype developed during the course of this work, is still has manageable size and may find some field applications.